SORPTION ENHANCED MIXED MATRIX MEMBRANES FOR HYDROGEN (H_2) PURIFICATION AND CARBON DIOXIDE (CO_2) CAPTURE

Final Report
Project Period: 9/1/2015 – 12/31/2019

by

Haiqing Lin, Ph.D. and Associate Professor
haiqingl@buffalo.edu
716-645-1856

Date Issued: April 23, 2020

The U.S. Department of Energy
Office of Fossil Energy,
National Energy Technology Laboratory
Award Number: DE-FE0026463

Department of Chemical and Biological Engineering
University at Buffalo, The State University of New York (UB)

Other Contributors:

University at Buffalo
Mark Swihart, Liang Huang, Leiqing Hu
Shaleish Konda, Abhishek Kumar, Hien Nguyen
Maryam Omidvar, Deqiang Yin, Lingxiang Zhu

Membrane Technology and Research, Inc.
Carlos Casillas, Jay Kniep

University of Kentucky
Landon Caudill, Kunlei Liu

DISCLAIMER

This report was prepared as an account of work sponsored by an agency of the United States Government. Neither the United States Government nor any agency thereof, nor any of their employees, makes any warranty, express or implied, or assumes any legal liability or responsibility for the accuracy, completeness, or usefulness of any information, apparatus, product, or process disclosed, or represents that its use would not infringe privately owned rights. Reference herein to any specific commercial product, process, or service by trade name, trademark, manufacturer, or otherwise does not necessarily constitute or imply its endorsement, recommendation, or favoring by the United States Government or any agency thereof. The views and opinions of authors expressed herein do not necessarily state or reflect those of the United States Government or any agency thereof.

Final Report
Covering Period: September 1, 2015 – December 31, 2019
Date of Report: March 31, 2020
Date Submitted: April 23, 2020
Revised Submission: August 5, 2020

Submitted to

Report Prepared for:	DOE NETL
Award Number:	DE-FE0026463
Project Title:	Sorption Enhanced Mixed Matrix Membranes for Hydrogen (H_2) Purification and Carbon Dioxide (CO_2) Capture
Technical Contact:	Dr./Prof. Haiqing Lin; haiqingl@buffalo.edu; 716-645-1856
Recipient Organization:	The Research Foundation for State University of New York 402 Crofts Hall, Buffalo, NY 14260
Project Period:	9/1/2015 – 12/31/2019
Signature:	
DOE Project Officer:	Isaac 'Andy' Aurelio U.S. Department of Energy National Energy Technology Laboratory Morgantown Campus 3610 Collins Ferry Road 304-285-0244 Isaac.Aurelio@netl.doe.gov
DOE Contract Specialist:	Raelynn Honkus U.S. Department of Energy National Energy Technology Laboratory Pittsburgh Campus 626 Cochrans Mill Road Raelynn.Honkus@netl.doe.gov

ABSTRACT

Membrane technology is an energy-efficient and low-cost approach for pre-combustion CO_2 capture and H_2 purification in the integrated gasification combined cycle (IGCC) processes. Conventional membranes are based on rigid polymers with strong size sieving ability, such as poly[2,2'-(m-phenylene)-5,5'-bisbenzimidazole] (PBI) that provides high H_2/CO_2 diffusion selectivity. In this project, we demonstrate enhanced H_2 sorption and diffusion in PBI films with embedded palladium (Pd) nanoparticles, which have a strong affinity towards H_2. Pd nanoparticles with uniform diameters of 6 - 8 nm are prepared via a hot-injection colloidal synthesis. The loading of Pd nanoparticles in PBI increases H_2 sorption by almost 1,000 times, and at high Pd loadings, the Pd nanoparticles may form fast channels allowing the H_2 molecules to jump from one particle to another and thus increasing the effective H_2 diffusivity. For example, adding 70 wt.% Pd in PBI increases H_2 permeability from 25 to 70 Barrers and H_2/CO_2 selectivity from 13 to 29 at 150 °C. Such performance is above the Robeson's upper bound for H_2/CO_2 separation, demonstrating the potential of these new materials for industrial H_2/CO_2 separation. We have also fabricated these nanocomposites into thin-film composite membranes with H_2 permeance of 500 gas permeance units (GPU) and H_2/CO_2 selectivity of 30 at 150-200 °C. These membranes will be the central component in the design of membrane-based systems for 90% capture of CO_2 from coal-derived syngas, with 95% CO_2 purity at a cost of electricity 30% less than baseline capture approaches. The membranes were also tested with raw syngas at University of Kentucky, demonstrating their stability.

TABLE OF CONTENTS

1. EXECUTIVE SUMMARY

The technical objective of this project was to develop sorption enhanced mixed matrix membranes with H_2 permeance of 500 gas permeance units (GPU) and H_2/CO_2 selectivity of 30 at 150-200 °C. These membranes will be the central component in the design of membrane-based systems for 90% capture of CO_2 from coal-derived syngas, with 95% CO_2 purity at a cost of electricity 30% less than baseline capture approaches. The unique approach in this proposal is to design crosslinked polymers containing Pd-based nanoparticles achieving strong H_2 sorption and size-sieving ability and thus H_2/CO_2 selectivity. The specific objectives for each budget period (BP) are described below.

BP 1: Identify polymer matrix with strong size sieving ability and palladium (Pd)-containing nanomaterials to prepare freestanding mixed matrix films with H_2 permeability of 50 Barrer and H_2/CO_2 selectivity of 30 at 150-200°C with simulated syngas.

BP 2: Prepare and optimize thin film mixed matrix composite membranes materials with H_2 permeance of 500 GPU and H_2/CO_2 selectivity of 30 at 150-200 °C, and complete the modification of the membrane test unit for the field test in the BP 3.

BP 3: Conduct a 20-day field test of the membranes with real syngas at Center for Advanced Energy Research (CAER) of the University of Kentucky (UKy).

During the BP2, we have successfully prepared thin-film composite (TFC) membranes based on mixed matrix materials (MMMs) containing Pd nanoparticles in polymers, and demonstrated their superior and robust performance for H_2/CO_2 separation at 150 – 225 °C.

1. Production of the Pd-based nanoparticles with a diameter of 4 nm has been scaled up to 200 mg/day.
2. We have prepared TFC membranes with H_2 permeance above 500 GPU and H_2/CO_2 selectivity above 30 at temperatures up to 225 ºC, which meet the targets for the BP2.
3. We have conducted parametric studies of TFC membranes with a mixed gas containing H_2S and H_2O and demonstrated the stability of the membranes.
4. We have established a new testing plan at the Center for Advanced Energy Studies (CAER) at the University of Kentucky because NCCC decided to shut down their gasifier.

During this project, four Ph.D. students received the inter-disciplinary training and graduated, including Shailesh Konda, Maryam Omidvar, Deqiang Yin, and Lingxiang Zhu. One postdoctoral researcher (Dr. Liang Huang) and two Ph.D. students (Abhishek Kumar and Hien Nguyen) are involved in this project.

The project leads to one provisional patent application, eight peer-reviewed articles, and one manuscript in preparation. The details are shown below.

2. INTRODUCTION AND OUR APPROACH

Introduction. One approach to controlling CO_2 emissions is to decarbonize fossil fuels before combustion and capture the CO_2 for utilization or sequestration.[1, 2] In this process, coal is gasified to produce syngas, *i.e.*, hydrogen (H_2) and carbon monoxide (CO). The CO is converted to CO_2 by the water-gas shift reaction, producing more H_2. The shifted syngas contains ~55% H_2 and ~40% CO_2 at 150-200ºC and 20-40 bar.[3] CO_2 must be removed from the syngas stream economically, to be utilized or sequestered with modest increase in energy costs.[1, 4] The current leading technologies for pre-combustion CO_2 capture are physical absorption processes, such as Selexol® or Rectisol®.[2] These processes are complex and consumes large amounts of energy in the absorber-stripper operation.

Membrane processes have previously been suggested as a means to lower the cost and energy intensity of IGCC syngas cleanup. Membrane processes for CO_2 capture must be integrated into the process trains to achieve the best possible energy efficiency. Much of this effort has focused on inorganic membranes because of the perceived desirability of operating at high temperatures.[5-7] Over the past decade, a large research effort has been expended on palladium alloy and other metallic membranes that selectively transport hydrogen at elevated temperatures. Membranes of this type offer the potential of process intensification in syngas cleanup by combining water-gas shift reactions with hydrogen separation.[7, 8] Despite this promise, there are significant hurdles to moving this technology beyond the laboratory. In the 1950s and 1960s, Union Carbide studied palladium alloy membranes extensively, even building a large demonstration plant for hydrogen separation. However, in the end, membrane cost and reliability issues made this technology uncompetitive with other separation techniques.[9] These practical problems persist today. Ongoing work seeks to reduce membrane cost by making thinner selective layer and using alloys with low cost metals, improve the membrane tolerance to sulfur species and other contaminants, and address module fabrication, reliability, and scale-up challenges.[10-15] Other inorganic materials such as ceramics[16, 17] are faced with similar challenge, *i.e.*, membrane scale-up and module fabrication. Nevertheless, no commercial inorganic membrane system for industrial gas separations has yet been installed or is in sight.

Membrane Process Designs. MTR had developed various process designs based on membranes. Figure 2 shows an example membrane design for H_2 purification and CO_2 capture from coal-derived syngas, using a H_2-permeable, CO_2-rejecting membrane for the main shift reactor gas separation, a CO_2-permeable, hydrogen-rejecting polymer membrane to concentrate CO_2, and a cryogenic unit for the production of liquid CO_2.[4, 18]

Figure 1 compares the power consumption of the membrane process and Selexol for CO_2 capture from the GE gasification syngas. In both cases, H_2 recovery and CO_2 capture rates are held constant at ~99% and 90%, respectively.[4, 18] The calculations show that with a base membrane with H_2 permeance of 300 GPU and H_2/CO_2 selectivity of 15, the CO_2 capture using the membrane process increases the LCOE by 15%. The membrane process can achieve the DOE goal of <10% LCOE increase using membranes with H_2 permeance of 900 GPU and H_2/CO_2 selectivity of 40. However, this would be a very ambitious goal. A more realistic goal, to be pursued in this project, was to develop membranes with H_2 permeance of 500 GPU, and H_2/CO_2 selectivity of 30, which, alone, will achieve a LCOE increase of ~12%. We expect that the

LCOE increase can be further reduced to 10% or less by optimizing the hybrid process designs, such as a better integration of the cryogenic unit and membrane unit, or an integration of the membrane with absorption unit.

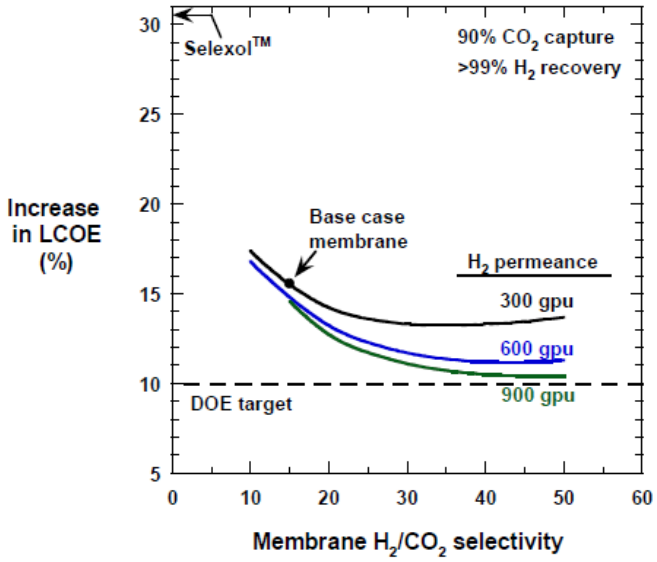

Figure 1. Comparison of power consumption for a membrane process with different H_2/CO_2 selectivities and the Selexol process for CO_2 capture from the GE IGCC process.[4, 18] Figure adapted from the literature.[4, 18]

Current Membrane Technology for H_2/CO_2 Separation. Polymer based membranes are much easier to implement, compared to inorganic membranes, provided that the membrane materials demonstrate suitable separation properties. Production scale up and module fabrication using polymeric membranes have been widely practiced creating substantial engineering know-how across the polymer membrane industry.[9] For H_2/CO_2 separation, diffusivity selectivity favors hydrogen, because hydrogen (with a kinetic diameter of 2.89 Å) is smaller than CO_2 (with a kinetic diameter of 3.3 Å), as shown in Table 1.[21] However, solubility selectivity favors CO_2 because CO_2 (with a critical temperature of 304 K) is much more condensable than hydrogen (with a critical temperature of 33 K).[21] The favorable H_2/CO_2 diffusivity selectivity is offset by the unfavorable solubility selectivity, so most polymeric materials do not show high H_2/CO_2 selectivity.[22-24] Current strategies to develop H_2-selective materials are often focused on enhancing the polymer size-sieving ability to increase H_2/CO_2 diffusivity selectivity. Due to the lack of specific interactions between H_2 and polymers, there has been very little work focused on enhancing H_2/CO_2 solubility selectivity to improve H_2/CO_2 separation properties.

Table 1. Physical properties of CO_2 and H_2 governing gas transport properties.[19, 20]

Gas	Kinetic diameter (Å)	Critical temperature (K)
H_2	2.89	33
CO_2	3.3	304

The key to enable the membrane based process for CO_2 capture is the development of improved H_2-selective and CO_2-rejecting membranes. Figure 5 presents a permeability/selectivity plot for H_2/CO_2 separation in polymeric membranes, where gas transport follows the solution-diffusion mechanism. This type of plot was popularized by Robeson.[21, 24, 25] Each point on the graph represents the separation characteristics of a specific material.[26-29] The upper bound line in the figure gives a rough estimate of the highest H_2/CO_2 selectivity possible for a given permeability

in polymer-based materials.[21, 25] A trade-off exists between gas selectivity and permeance; that is, materials with higher H_2 permeance have lower H_2/CO_2 selectivity. This is also exemplified by the series of polyimides crosslinked with diamines, which show increasing H_2/CO_2 selectivity and decreasing H_2 permeance with increasing crosslinking density.[30, 31]

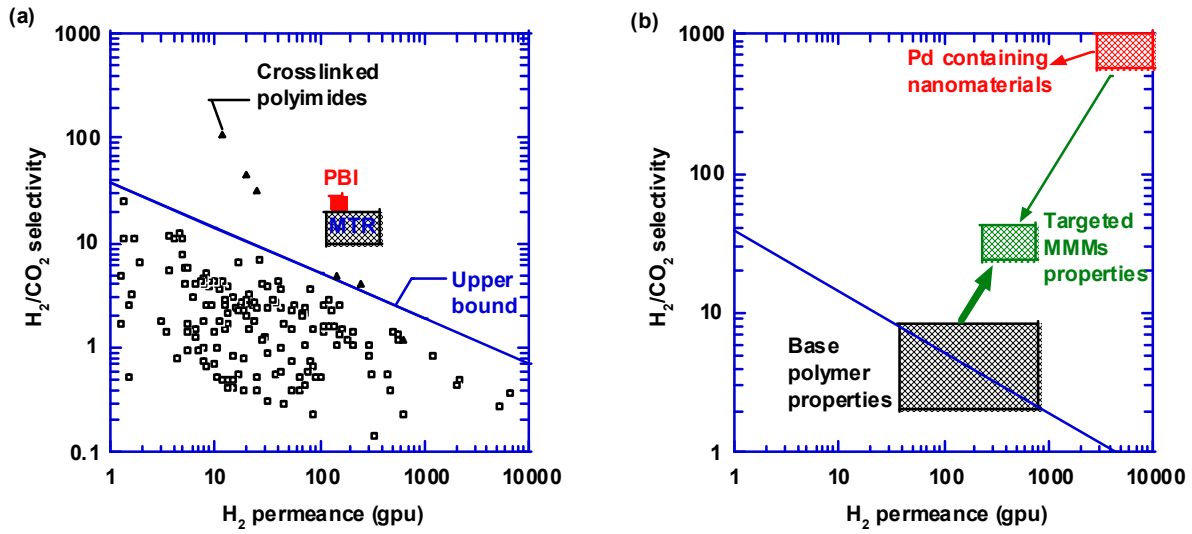

Figure 2. (a) Upper bound of H_2/CO_2 separation using polymeric membranes at 25°C.[24] The data for the upper bound and crosslinked polyimides (35°C)[28, 29, 31] were estimated based on a thin film thickness of 1 μm. The PBI data were obtained at 250°C for hollow fiber membranes.[26, 27, 32, 33] (b) Rationale of using Pd-based nanomaterials for mixed matrix membranes for H_2/CO_2 separation.

DOE has been funding initiatives aimed at developing new membrane-based technologies for carbon capture from IGCC syngas. A group led by Los Alamos National Laboratory and SRI International has investigated high-temperature hydrogen-selective polymeric membranes such as polybenzimidazole (PBI), which exhibit attractive H_2/CO_2 selectivities at operating temperatures of 200–300°C.[26, 27, 32, 33] The chemistry of PBI makes these materials difficult to fabricate into the extremely thin, high-surface-area membranes required for an industrial system. Ongoing work is focused on improving the permeance (throughput) of the membranes and developing ways to process the PBI materials into an industrially viable membrane module.

Funded by DOE/NETL, Membrane Technology and Research, Inc. (MTR) has also been developing Proteus™ membranes for H_2/CO_2 separation at temperatures up to 150°C.[4, 18] The membrane stamps have been extensively evaluated in the laboratory using simulated syngas, and at NCCC using real syngas. As shown in Figure 5, the Proteus membranes exhibit permeance of 100-300 GPU and H_2/CO_2 selectivity of 15-20.[4, 18] Ongoing effort is focused on the scale up of membrane and module production, and pilot-scale demonstration of the membrane processes.

Other research efforts on development of new membrane materials, such as graphene based membranes[34, 35] and mixed matrix membranes containing metal organic frameworks (MOFs)[36] are also ongoing. These new materials are tailored to enhance the size-sieving ability of the

materials, increasing H_2/CO_2 diffusivity selectivity and thus permeability selectivity. While these materials have shown interesting properties, they are at an early stage of development, and the fabrication of these materials into layers of less than 100 nm with well-controlled morphology to achieve high H_2/CO_2 diffusivity selectivity remains a grand challenge.

In summary, the current polymeric membrane materials rely solely on the strong size sieving derived from the rigid polymer chains, which inevitably leads to low H_2 diffusion coefficient and low H_2 permeability. This proposed work adopts a completely different approach by focusing on enhancing H_2 solubility and H_2/CO_2 solubility selectivity to overcome the permeability/selectivity trade-off.[22, 37]

Our Approach and Rationale for Developing Sorption Enhanced Mixed-Matrix Membranes. Optimal membrane materials for H_2/CO_2 separation must have

- strong affinity towards H_2 at elevated temperatures, to achieve reversibly high H_2 solubility and H_2/CO_2 solubility selectivity; and
- strong size-sieving ability to achieve high H_2/CO_2 diffusivity selectivity.

Our approach to overcome the inherent roadblocks to simultaneously attaining high permeability and selectivity in polymers consists of starting with strongly size-sieving polymers and adding Pd-based nanomaterials to increase both permeability and selectivity into a range suitable for commercial deployment. Palladium exhibits extremely high H_2 sorption. For example, Pd can sorb 0.56 wt% hydrogen at 25°C and 0.02 bar, while most polymers may sorb only 10^{-5} wt% H_2 under the same conditions.[38] Therefore, the addition of Pd nanoparticles into the polymers can tremendously increase H_2 sorption in the nanocomposites. As a result, Pd-based nanomaterials including nanoparticles and metal organic frameworks containing Pd or Pd^{2+} have been explored as H_2 storage materials.[39-41] For example, according to quantum-mechanical (QM) calculations, the incorporation of $PdCl_2$ into a porous polymer (covalent organic framework) leads to an extremely high H_2 sorption of 6.0 wt% at 298K and 100 bar, which is ascribed to the favorable interactions between the Pd sites and H_2.[40, 42]

Table 2 directly shows the vastly superior H_2 sorption capacity in Pd metal in comparison with conventional polymers considered for membrane gas separation. For example, polysulfone and Matrimid are typical glassy polymers with strong size sieving ability; PDMS has the lowest glass transition temperature among polymers known; PTMSP and Teflon AF are glassy polymers with very high free volume. Most of these polymers show H_2/CO_2 solubility selectivity of less than 0.2, which is much less than that in the Pd metal with H_2/CO_2 solubility selectivity of > 1000.[13] If nanomaterials containing Pd or Pd^{2+} can be tailored in the mixed matrix membrane materials, we expect that such membranes can have much higher H_2 solubility and permeability, and higher H_2/CO_2 selectivity compared to polymers.

Table 2. Highlight of extraordinary H_2 solubility and H_2/CO_2 solubility selectivity in Pd metals compared with polymers considered for gas separations.

Materials	Temp. (°C)	H_2 solubility $cm^3(STP)/(cm^3\ atm)$	H_2/CO_2 solubility selectivity	Ref.
Poly(dimethyl siloxane)	35	0.10	0.078	43, 44
Polysulfone	35	0.075	0.036	43, 45
Matrimid®	35	0.12	0.035	43, 46
Teflon AF2400	35	0.21	0.13	43, 47
Poly(1-(trimethyl-silyl) propine) (PTMSP)	35	0.40	0.11	48
Pd metal*	**25**	**38,000**	**> 1,000**	13, 38

* The value of H_2 sorption in Pd was calculated from the data at H_2 pressure of 0.02 bar.

Furthermore, if the Pd-based nanomaterials can be incorporated into the polymer matrix at sufficiently high loading, the sorbed H_2 may diffuse through the membrane by a hopping mechanism, enhancing H_2 diffusivity and increasing H_2 permeability and H_2/CO_2 selectivity, as shown in the left panel of Figure 3.[49, 50] Moreover, networks of the Pd-based nanomaterials in the form of nanowires or fractal aggregates of nanoparticles can form percolated networks, contributing to high H_2 diffusivity and thus permeability, as shown in the right schematic of Figure 3.

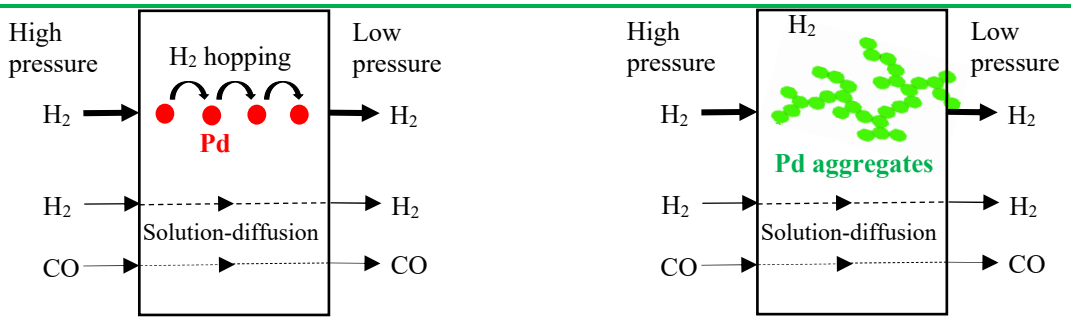

Figure 3. (Left) Schematic of enhanced H_2 sorption and diffusion due to the Pd-based nanomaterials, which leads to H_2 molecule hopping and thus high H_2 diffusivity in the membrane. (Right) schematic of enhanced H_2 sorption and diffusion due to fractal aggregates of Pd-based particles, which provide a channel for H_2 diffusion.

We proposed to achieve strong size sieving ability using the leading materials for H_2/CO_2 separation, polybenzimidazole (PBI), as shown in Figure 2a. These polymers have already shown H_2 permeance of 100-200 GPU and H_2/CO_2 selectivity of 10-20, as shown in Figure 2. If the addition of Pd-based nanomaterials enhances the H_2 solubility by 2-3 times, the mixed matrix membranes are expected to exhibit H_2 permeance of 500 GPU and H_2/CO_2 selectivity of 30.

Our approach to developing mixed matrix membranes (MMMs) drastically differs from prior studies in the literature. Many MMMs have been proposed for O_2/N_2, CO_2/CH_4 and H_2/CO_2 separations.[51-54] The first generation MMMs are often based on zeolites with well-controlled pore size and strong size sieving ability achieving high diffusivity selectivity.[55] However, zeolite particles typically have a size of microns, and the processability of MMMs into membranes of

~100 nm thickness is daunting. The second-generation membranes are based on metal-organic frameworks (MOFs) with pore sizes between the sizes of the two gas molecules to be separated.[56-59] The MOF particles can be less than 100 nm and therefore, they can potentially be processed into thin film.[36] These MMMs rely on the size sieving ability of the nanoparticles and therefore, the compatibility of MOFs with polymers, and the effect of water vapor blocking in the pores on gas separation properties need to be considered. On the other hand, our approach here does not rely on the size sieving from the Pd-based nanomaterials. Therefore, the pore blocking will not reduce the gas permeances in these membranes to be developed, and the membrane separation performance will not depend sensitively on the nanostructures in the membranes.

3. PROJECT MANAGEMENT AND PLANNING

Table 3 summarizes the milestones designed to evaluate the progress of the project. We had fully met the milestones and targets, and the timelines are also shown in Table 3. The detailed technical achievements are shown below.

Table 3. Overview of project milestone status.

Milestone Title/Description	Planned Completion Date	Actual Completion Date	Verification Method
Updated Project Management Plan	11/30/2015	9/23/2015	Project Management Plan file
Kickoff Meeting	12/31/2015	10/5/2015	Presentation file
Final report	11/30/2018	N/A	Report file
Polymers and nanomaterials with promising H_2/CO_2 separation properties identified and prepared	6/30/2016	6/30/16	Materials
Mixed matrix materials with superior H_2/CO_2 separation properties prepared	9/30/2016	9/30/2017	Separation property data
Mixed matrix membranes with superior H_2/CO_2 separation properties	12/31/2017	3/31/2018	Separation property data
Field test unit modified	5/31/2018	10/31/2019	Test system
Successful field test	11/30/2018	12/31/2019	Field data

4. DEVELOPMENT OF MEMBRANE MATERIALS WITH H_2 PERMEABILITY OF 50 BARRER AND H_2/CO_2 SELECTIVITY OF 30

Figure 4a depicts sorption-enhanced MMMs incorporating Pd nanoparticles (NPs) in PBI to achieve high H_2 permeability and H_2/CO_2 selectivity simultaneously. Sub-10 nm Pd particles were synthesized by reducing Pd(II)acetylacetonate in oleylamine (OAm) and borane tributylamine complex. The obtained Pd NPs are coated with 7.8 wt.% OAm ligands through the

strong interaction between the amine groups and Pd, determined by thermal gravimetric analysis (TGA). The OAm improves the dispersibility of the Pd NPs and mitigates their aggregation. However, it is not expected to interact with PBI or improve the compatibility of the Pd NPs and PBI. Figure 4b displays transmission electron microscopy (TEM) images of Pd NPs (diameter: 4.6 ± 0.5 nm). Their selected area electron diffraction (SAED) pattern (Figure 1c) demonstrates they are polycrystalline, as further confirmed by x-ray diffraction (XRD).

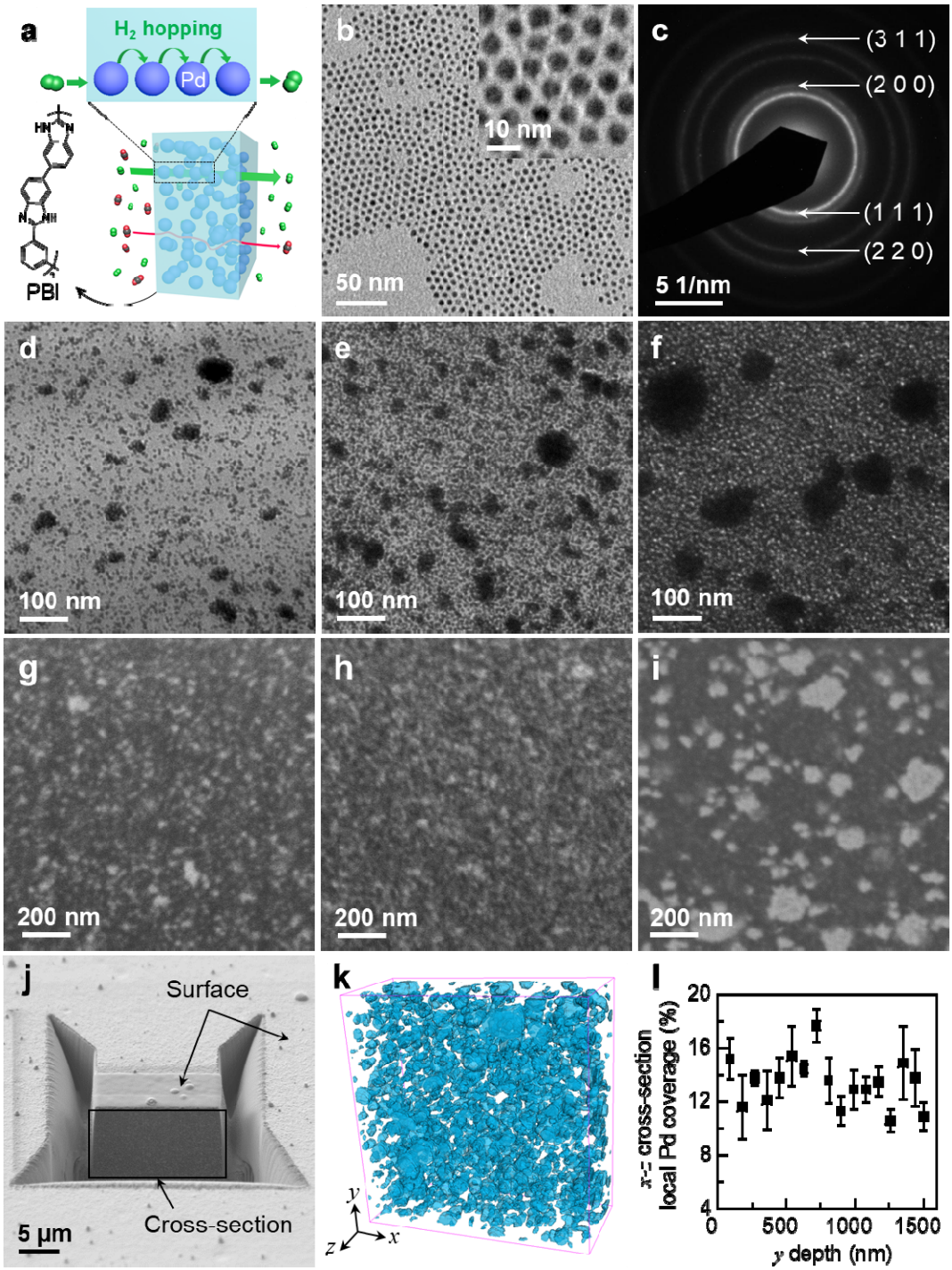

Figure 4. Design, synthesis, and characterization of PBI-Pd MMMs. a) Schematic of H_2 hopping among Pd NPs in the PBI matrix. b, c) TEM images (b) and SAED pattern (c) of Pd NPs. d-i) Cross-sectional TEM images (d, e, f) and cross-sectional SEM images (g, h, i) of PBI-Pd-22/2.9 (d, g), PBI-Pd-46/8.1 (e, h), and PBI-Pd-58/12 (f, i). Pd appears dark and light in TEM and SEM images, respectively. j) U-shaped trench with a frame highlighting a selected region for FIB-SEM cross-sectional imaging and further 3D tomography analysis. k) Surface-rendered view of reconstructed 1500:1500:650(*x*:*y*:*z)* nm volume for PBI-Pd-58/12. Pd is blue, and PBI is transparent. l) Pd coverage in *x*-*z* cross-section *versus* film depth of PBI-Pd-58/12.

Freestanding MMM films of PBI-Pd-*a*/*b* were fabricated by solution casting, where *a* and *b* represents the weight and volume percentage of the Pd NPs, respectively. PBI and Pd content were determined by TGA. For example, a PBI-Pd-58/12 indicates a Pd content of 58 wt.% or 12 vol.%. The 12 vol.% Pd content is the maximum Pd loading to obtain defect-free MMM films in this study. Cross-sectional TEM images (Figure 4d, e, and f) and SEM images (Figure 4g, h and i) show that the NPs are well dispersed in the MMMs, though a few aggregates (<100 nm) are observed in PBI-Pd-22/2.9 and PBI-Pd-46/8.1, and more aggregates (100 – 200 nm) appear in PBI-Pd-58/12. Single Pd NPs are distinguishable in the SEM image of PBI-Pd-58/12, in contrast to the TEM image. Dispersion of NPs among PBI chains somewhat disrupts their π-π stacking and short-range order, as indicated by XRD analysis, due to Pd NP interactions with amine groups of PBI.

Focused ion beam scanning electron microscopy (FIB-SEM) tomographic reconstruction of the 3D nanostructure of PBI-Pd-58/12 provides further insight.[17] A U-shaped trench was carved to expose sequential cross-sections (Figure 4j), and 325 consecutive images were recorded within a 1500×1500×650 nm^3 volume. The 3D nanostructure was reconstructed and shown in Figure 4k with Pd in blue and transparent PBI. Figure 4l depicts cross-sectional Pd coverage over a depth of 1500 nm along the gas transport direction (*y*-axis) at 90 nm intervals. The Pd nanoparticles occupy the sample cross-section uniformly at all depths with an average coverage of 13.5 ± 2.3%. No voids were observed, indicating the compatibility of PBI and the OAm-coated Pd NPs. Compatibility was also confirmed macroscopically by density measurements showing that the MMM density is 2 - 5 % higher than the values estimated using an additive model.

H_2 sorption isotherms in Pd NPs and MMMs at 150 °C and pressures of 0.1 - 1.3 bar (Figure 5a) show formation of α-phase PdH_x (x = 0.10 at 1.3 bar) and then β-phase PdH_x (x = 0.40 at 1.5 bar), as expected. At H_2 pressures above 2 bar, Pd exhibits an impressive H_2 saturation sorption of 700 ± 22 cm^3 (STP) cm^{-3} (x = 0.55). H_2 sorption increases linearly with increasing Pd content in MMMs, indicating the negligible effect of the OAm on the H_2 sorption. At 10 bar, PBI-Pd-58/12 sorbs 10.3 ± 0.3 cm^3 (STP) cm^{-3} atm^{-1} H_2, three orders of magnitude more than typical glassy polymers such as Matrimid and polysulfone (~0.07 cm^3(STP) cm^{-3} atm^{-1} at 70 °C). CO_2 sorption in the MMMs (Figure 5b) follows a dual-mode sorption model with fitting parameters. CO_2 cannot access Pd NPs, and thus sorption decreases linearly with Pd content, further enhancing H_2/CO_2 solubility selectivity. The H_2/CO_2 solubility selectivity of PBI-Pd-58/12 (28 ± 1 at 10 bar and 150 °C) exceeds that of typical polymers (*ca.* 0.01) by more than 3 orders of magnitude.

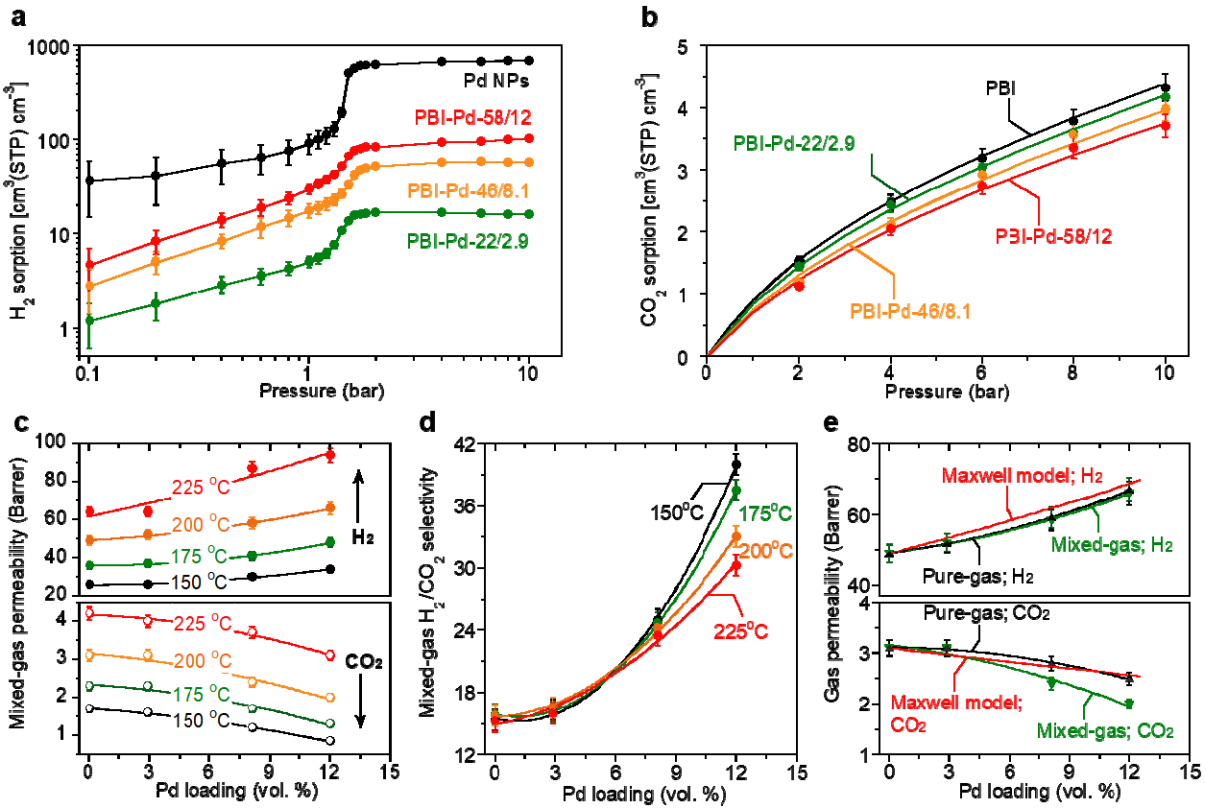

Figure 5. Gas sorption and transport in PBI-Pd MMMs. a, b) H_2 (a) and CO_2 (b) sorption isotherms at 150 °C, and the curves are best fits of the dual-mode sorption model. c, d) Mixed-gas H_2 permeability (c) and H_2/CO_2 selectivity (d) *versus* Pd loading in vol.%. e) Comparison of experimental and predicted pure- and mixed-gas permeability at 200 °C. Red curves show pure-gas permeability from the Maxwell model.

Figure 5c shows that increasing Pd loading increases H_2 permeability and decreases CO_2 permeability at 150 – 225 °C in a 50% H_2/50 CO_2% mixture at 10 bar, leading to an increase in the mixed-gas H_2/CO_2 selectivity (Figure 5d). The simultaneous increase in H_2 permeability and H_2/CO_2 selectivity can be ascribed to the improved H_2 sorption and H_2/CO_2 solubility selectivity, which is an effective method to break the permeability/selectivity tradeoff. Both H_2 permeability and H_2/CO_2 selectivity improve significantly as the Pd content increases from 8.1 to 12 vol.%. This coincides with increased electrical conductivity, which is three orders of magnitude higher for PBI-Pd-58/12 (36 ± 4 S m^{-1}) than for PBI-Pd-46/8.1. Pd NPs in PBI-Pd-58/12 may have formed chains or aggregates that span the film and facilitate both electrical conduction and H_2 transport.

As the temperature increases from 150 to 225 °C, gas permeability increases significantly with the activation energy for permeation of 22 ± 2 and 25 ± 4 kJ mol^{-1} for H_2 and CO_2, respectively, presumably because the MMMs contain 88 vol.% PBI or higher. As shown in Figure 5d, the H_2/CO_2 selectivity in all the examples remains almost constant at various temperatures except for PBI-Pd-58/12, which shows a slight decrease in the selectivity with increasing temperature. PBI-Pd-58/12 has a high content of flexible OAm ligands (4.9 wt.% or 15 vol. %), which may decrease the size-sieve ability of MMMs at higher temperatures. Nevertheless, PBI-Pd-58/12 still

exhibits better selectivity than any other samples at any temperature range. For example, adding 12 vol% Pd in PBI increases mixed-gas H_2 permeability from 63 to 94 Barrer and mixed-gas H_2/CO_2 selectivity from 15 to 30 at 225 °C.

Figure 5e compares mixed- and pure-gas permeability of MMMs at 10 bar and 200 °C. Pure- and mixed-gas H_2 permeabilities are identical, but mixed-gas CO_2 permeability is lower than pure-gas values for the MMMs. This effect increases with Pd loading, further enhancing H_2/CO_2 mixed-gas selectivity. The same effect was observed at 150, 175, and 225 °C. Reduced mixed-gas CO_2 permeability may arise from swelling of Pd NPs upon H_2 sorption, densifying the PBI matrix and decreasing CO_2 diffusivity. Figure 5e shows that pure-gas transport properties of MMMs are described by the Maxwell model.

Industrial H_2/CO_2 mixtures or coal-derived shifted syngas (typically ~56% H_2, ~41% CO_2) generally contain H_2O and trace H_2S. Adding 5 ppm H_2S to the dry feed slightly decreased H_2 permeability (from 48 to 43 Barrer) and H_2/CO_2 selectivity (from 37 to 31) of the MMMs (Figure 6a), as H_2S formed sulfides on Pd NPs, partially blocking H_2 dissociation. Unlike Pd-based metallic membranes that exhibited sharp (~75%) and instantaneous loss in H_2 permeability when exposed to ppm-level H_2S, this MMM exhibits only 14% permeability loss in H_2S, due to the high surface area of the Pd NPs. The separation performance remained constant for t = 32 – 48 h with H_2S, t = 48 – 96 h without H_2S, and t = 96 – 120 h with 0.4 mol% H_2O. Additionally, the XRD results confirm the integrity of the Pd NP crystalline structure for such a 120-h test at 175 °C, though the Pd NPs may be chemically active.

The Robeson's 2008 upper bound represents a tradeoff between H_2 permeability and H_2/CO_2 selectivity and defines the highest H_2/CO_2 selectivity achieved for any H_2 permeability in polymers at around 35 °C. Figure 6b benchmarks the mixed-gas H_2/CO_2 separation performance of PBI-Pd MMMs and Proteus™ membrane, which is a leading commercial membrane for H_2/CO_2 separation, in a Robeson's upper bound plot. Our MMMs, operating at 200 °C, are significantly above 2008 upper bound empirically drawn for 35 °C, another upper bound predicted for 200 °C, and even the performance of Proteus™ membranes, indicating their superior H_2/CO_2 separation performance. Increasing Pd content shifts MMMs' separation performance away from the upper bounds and toward the favorable performance region of the Robeson's plot.

Figure 6b compares H_2/CO_2 separation performance of PBI-Pd MMMs with other state-of-the-art materials like MMMs made of MOFs and Pd, and polymers such as Proteus™, polyamide, acid doped PBI, and PBI derivatives. Our PBI-Pd MMMs, far above the upper bounds, exhibit better separation performance than those polymers and the other MMMs, all of which are below or close to the upper bound predicted for 200 °C.

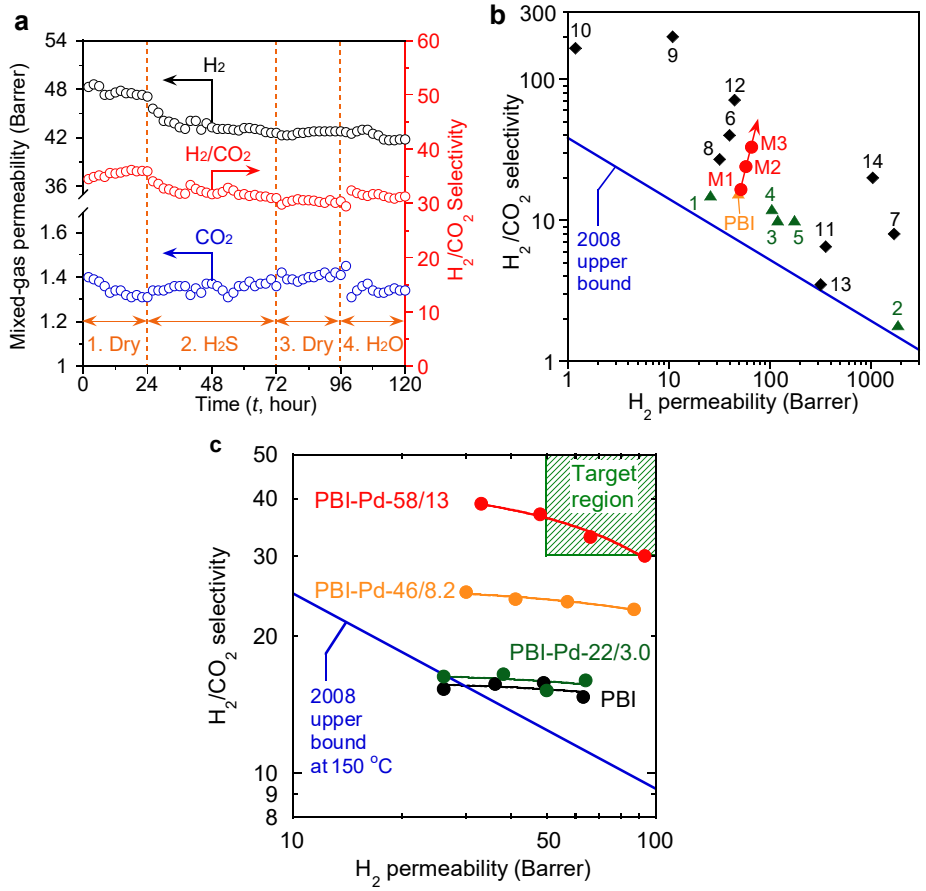

Figure 6. (a) Stability test of 10 μm thick PBI-Pd-58/12 film in H_2/CO_2 mixtures containing H_2S and H_2O at 175 °C and 10 bar. Conditions #1 and #3 (dry) used 50% H_2/50% CO_2, while condition #2 (H_2S) included 5 ppm H_2S, and condition #4 (H_2O) included 0.4 mol% water vapor. (b) Mixed-gas separation performance of PBI-Pd MMMs (M1: PBI-Pd-22/2.9, M2: PBI-Pd-46/8.1, and M3: PBI-Pd-58/12) at 200 °C *versus* Robeson's 2008 upper bound (the blue line) at 35 °C[21] and the only commercially available H_2/CO_2 separation membrane (Proteus™) to date.[22] (c) Demonstration of H_2/CO_2 separation properties in the MMMs that meet the target (H_2 permeability of 50 Barrer and H_2/CO_2 selectivity of 30).

Figure 6c compares the H_2/CO_2 separation properties in the MMMs with the targeted properties set in this project. The gas mixture contains 50% H_2 and 50% CO_2. Increasing the temperature from 150 ºC to 225 ºC for the MMMs containing 58 wt% Pd NPs (or 13 vol%) increases the H_2 permeability with a slight decrease in the H_2/CO_2 selectivity. The MMMs exhibit an H_2 permeability of 90 Barrer and H_2/CO_2 selectivity of 30 at 225 ºC, which meets the targets for the BP1 (MMMs with an H_2 permeability of 50 Barrer and H_2/CO_2 selectivity of 30).

5. DEVELOPMENT OF MEMBRANES WITH H_2 PERMEANCE OF 500 GPU AND H_2/CO_2 SELECTIVITY OF 30

The membrane configuration and performance have been summarized in Appendix A and B State of Data Point for Membrane Systems.

TFC membranes based on PBI-Pd MMMs. Industrial TFC membranes are often comprised of a selective layer on top of a microporous support and a gutter layer (such as polydimethylsiloxane or PDMS) to eliminate the geometric restriction from the porous support, as shown in Figure 7a.[60, 61] The first step in this study was to prepare a PBI microporous support stable at 150 – 250 °C via a phase inversion method on a stainless steel mesh cloth with superior mechanical strength. Figure 7b shows the SEM photo of the surface of the porous PBI support with a pore diameter of about 14 nm and surface porosity around 16%. At room temperature (23 °C), it has an H_2 and CO_2 permeance of 410,000 and 110,000 GPU, respectively, showing its negligible resistance for gas transport. Figure 7c presents the cross-sectional SEM photo of the TFC membranes comprising PBI-Pd-58/12 (800 ± 40 nm) and a gutter layer of plasma-etched PDMS (400 ± 20 nm).

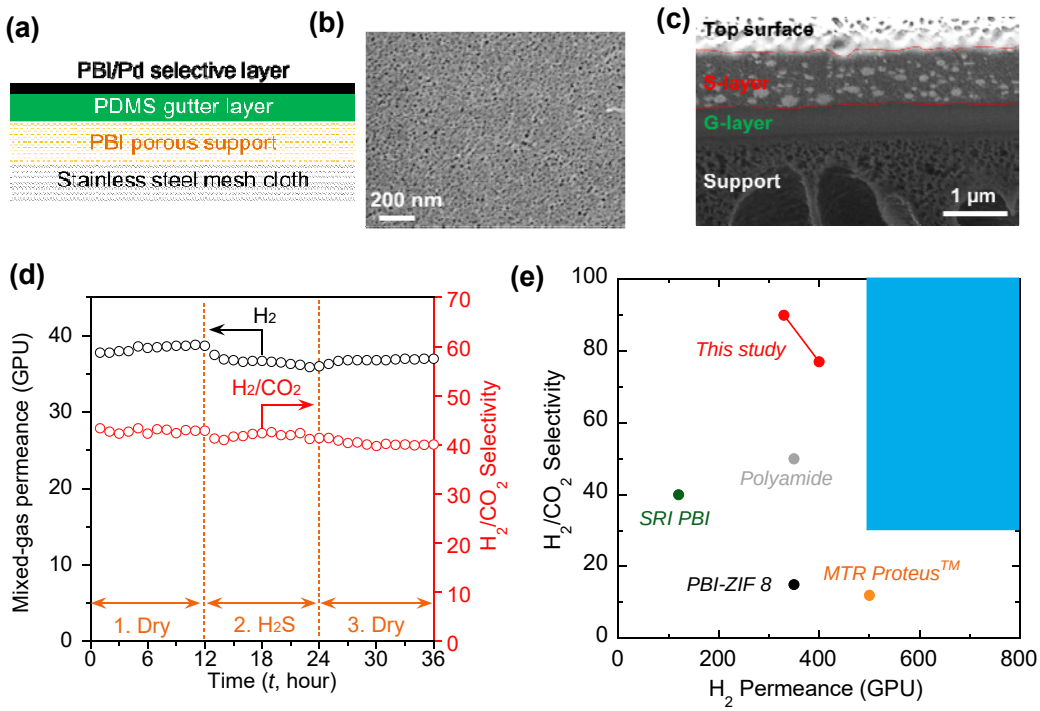

Figure 7. (a) Schematic illustration of TFC membranes comprising a PBI/Pd selective layer. (b) SEM images of the surface of a PBI-based porous support membrane. (c) Cross-sectional SEM image of the TFC membrane comprising a thin MMMs layer. (d) Stability test of a TFC membrane comprising an 800 nm-thick PBI-Pd-58/12 selective layer in H_2/CO_2 mixtures containing H_2S and H_2O at 175 °C and 10 bar. Conditions #1 and #3 (dry) used 50% H_2/50% CO_2, and condition #2 (H_2S) included 5 ppm H_2S. (d) Comparison of the TFC membrane based on 70 nm PBI-Pd-58/12 with other membranes for H_2/CO_2 separation.

The resulting TFC membrane exhibits H_2 permeance of 39 GPU and selectivity of 43 when tested with a dry binary mixture (50% H_2 and 50% CO_2) at 175 °C (Figure 7d). The intrinsic H_2 permeability (50 Barrer) and selectivity (43) exceed those of the bulk film (48 Barrer and 37), because continuous Pd NP chains (or H_2 fast transport pathway) can more readily span an 800

nm supported film than a 10 μm bulk film. Adding 5 ppm H_2S in the feed gas has a negligible effect on the H_2 permeance and selectivity, consistent with the bulk film results. The successful fabrication of the TFC membranes confirms the sufficient mechanical properties of these MMMs.

Figure 7d compares a TFC membrane comprising 70 nm PBI-Pd-58/12 with other membranes for H_2/CO_2 separation. Our TFC membrane exhibit a H_2 permeance of 330 GPU and H_2/CO_2 selectivity of 90 at 150 ºC, and a H_2 permeance of 400 GPU and H_2/CO_2 selectivity of 77 at 230 ºC. We expect that further increase in the temperature can increase the H_2 permeance to 500 GPU while retaining H_2/CO_2 selectivity of above 30. However, due to the temperature limit in the oven, we cannot achieve the temperature above 230 ºC.

The cost of Pd (≈$42 per gram currently) does not significantly increase the cost of membrane systems. For example, 1 m^2 TFC membrane based on 200-nm PBI-Pd-58/12 only uses 0.29 g Pd (or $12), while the cost of typical membrane systems is $500 – 1,000/$m^2$ membrane area, including modules, vessels, piping, instrumentation, etc.

Organosilica Membranes Based on PBI-Pd MMMs. During the process of preparing PBI-Pd based TFC membranes, we accidentally discovered a new type of membranes. When the PDMS layer was exposed to plasma to improve surface hydrophilicity, we produce a silica-like structure (or organosilica) at room temperature.[62, 63] Oxygen plasma effectively breaks organic bonds and removes C and H in the form of H_2O, CO_2, and low molecular weight hydrocarbons at ambient temperature, leaving a significant fraction of Si bonded to three or four oxygen atoms on the surface. The formation of this dense silica-like layer significantly improves the size-sieving ability of PDMS at the expense of reducing its gas permeability.[62, 64, 65]

Figure 8a reveals the reaction occurring on the PDMS surface in the presence of plasma oxygen species like O+, O-, O, O_2, and O_3. In the scheme, hydroxyl (C-OH), silanol (Si-OH) groups and interchain bonds (i.e., Si(-O_3) or Si(-O)$_4$) are produced after oxidation and scission of methyl groups, and the resulting structures and chemical compositions depend on plasma conditions such as power, oxygen pressure, and treatment time.[64, 66] As shown by x-ray photoelectron spectroscopy (XPS), the O/Si ratio increases along with a vast drop in the C/Si ratio (cf. Figure 8b), confirming the oxidation and methyl scission reactions on the PDMS surface. The high O/Si ratio close to 2 indicates the formation of a significant fraction of SiO_2 on the PDMS surface.

Figure 8c compares Si 2p XPS spectra of the pristine PDMS and representative organosilica samples (POSix, where x denotes the plasma exposure time in seconds). Increasing the plasma exposure time decreases the amplitude of Si(-O)$_2$ peak but significantly increases SiO_2 peak intensity. XPS depth profiling technique was employed to determine the thickness of the organosilica layer for the POSix samples. Figure 8d plots the O/Si ratio of specimens as a function of the depth profiling time and etch depth. The O/Si ratio of POSi360 decreases from 1.98 at its surface to 1.02 at 25-nm depth, indicating this sample has a 25 nm thick organosilica layer. In the same approach, the thickness of the silica layer of POSi120 and POSi15 was determined to be 25 nm and 19 nm, respectively. Figure 8e also shows a schematic of the surface of silica structure for POSi360.

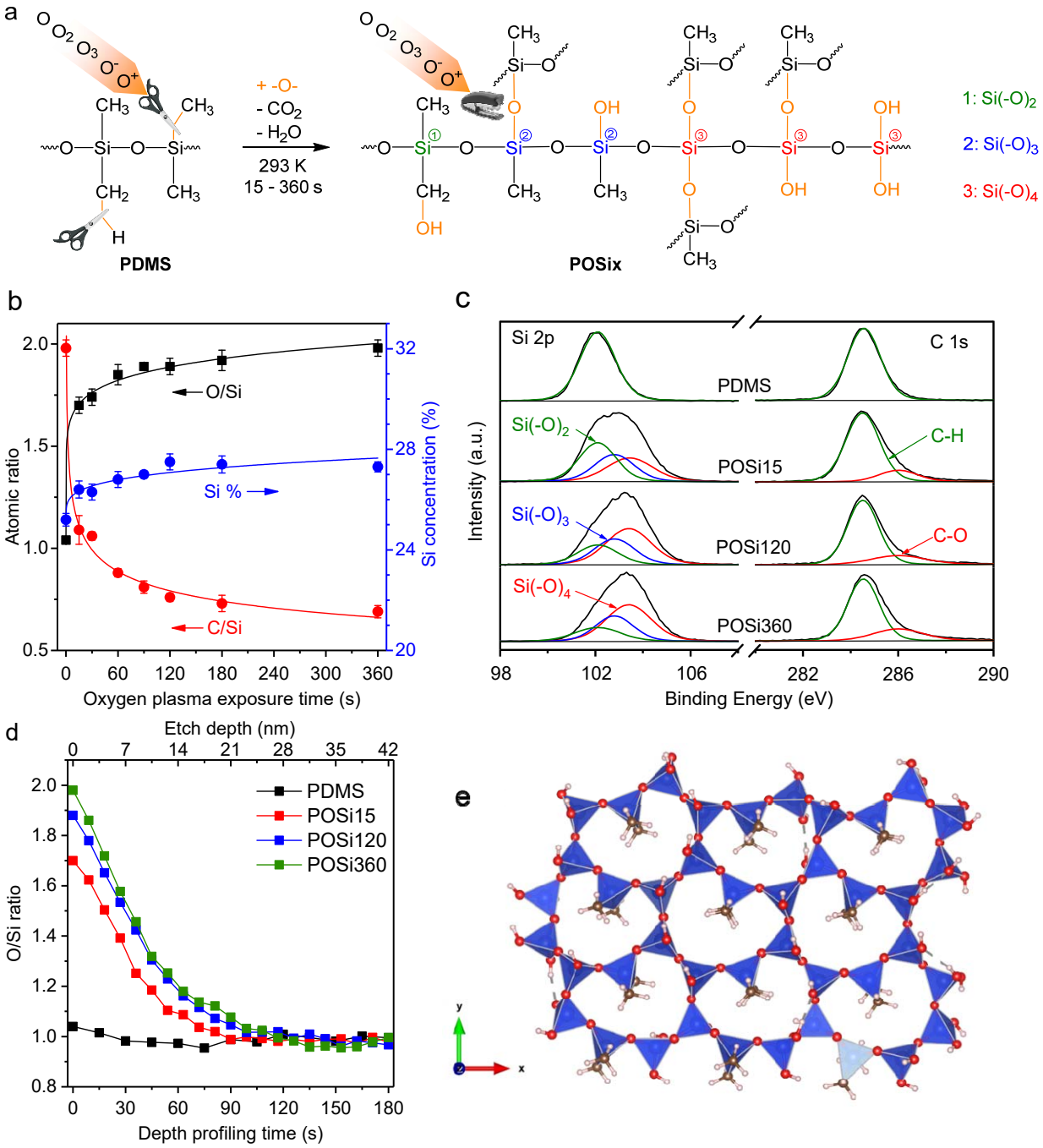

Figure 8. (a) Oxidation and crosslinking of PDMS in the presence of oxygen plasma. (b) Effect of oxygen plasma exposure time on Si concentration and C/Si and O/Si ratios on the PDMS surface. (c) Si 2p and C 1s XPS spectra and (d) XPS depth profiling of PDMS and plasma-treated PDMS samples (POSi15, POSi120, and POSi360). (e) Schematic structure of silica structure.

We conduct permeation tests with various gas molecules to probe pore sizes of the POSi120 at 150 ºC. As shown in Figure 9a, H_2 permeates 77 times as fast as CO_2, though their kinetic diameter difference is only 0.41 Å, suggesting that most pores for gas permeation in POSi120

may have a size between 2.89 Å and 3.3 Å. We investigated the mixed-gas separation performance of POSi TFC membranes using a binary gas mixture of 50% H_2 and 50% CO_2 at 150 °C with a feed pressure of 6.8 atm. Figure 9b displays that increasing the oxygen plasma exposure time decreases the mixed-gas permeance but significantly enhances H_2/CO_2 selectivity. Figure 9c shows that increasing the temperature drastically increases H_2 permeance and H_2/CO_2 selectivity.

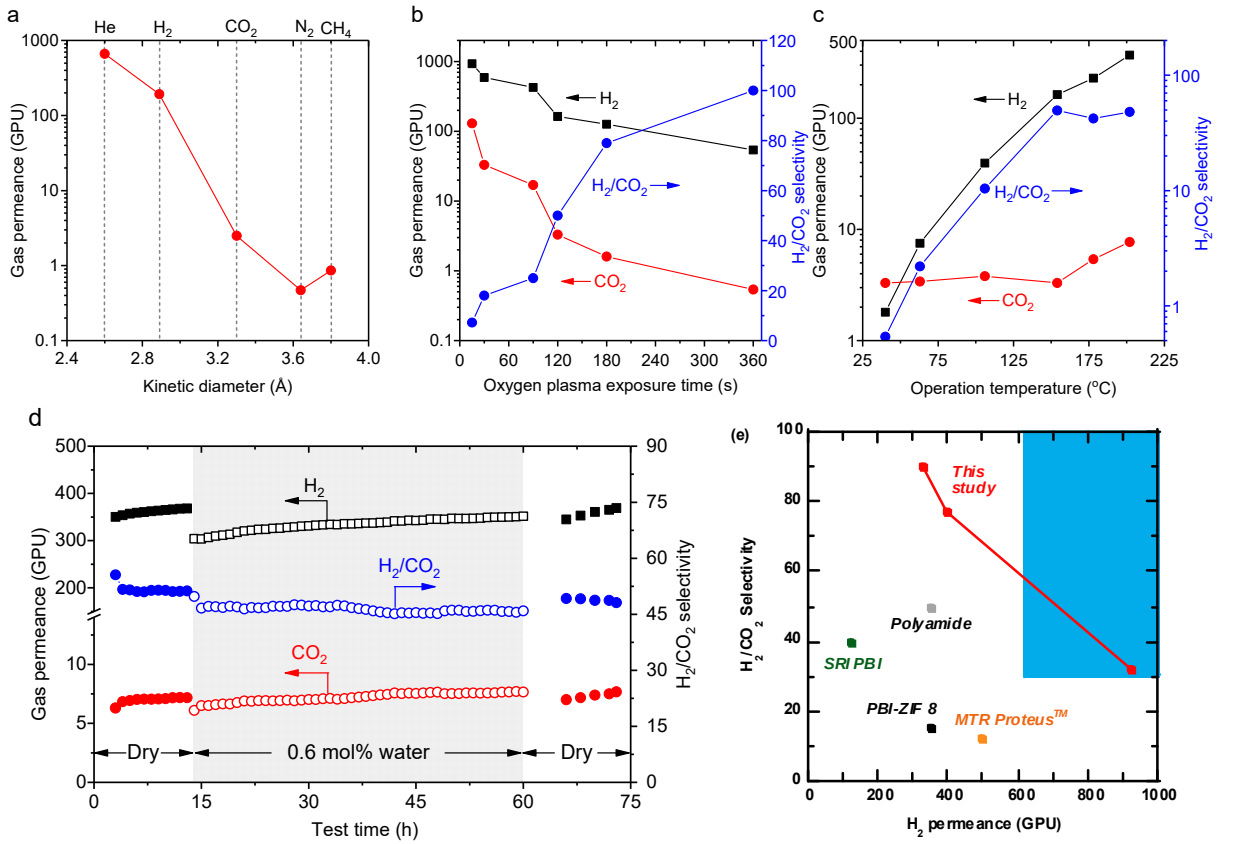

Figure 9. (a). Gas permeance of POSi120 uTFC membranes at 150 ºC. (b). Effect of oxygen plasma exposure time on gas separation performance of uTFC membranes at 150 ºC. c. Gas permeance and selectivity of a POSi120 uTFC membrane at various operating temperatures. The feed gas contains 50% H_2 and 50% CO_2 at 6.8 atm. d. Stability test of a POSi120 uTFC membrane with and without water vapor at 200 ºC. e. Comparison of separation performance of organosilica uTFC membranes with other membranes.

Figure 9d shows the effect of water vapor on mixed-gas separation properties and long-term stability of a POSi120 TFC membrane at 200 °C. The introduction of water vapor slightly decreases mixed-gas H_2 permeability from 370 GPU to 350 GPU and the H_2/CO_2 selectivity from 51 to 46. When the feed gas was shifted back to the dry binary mixture, the H_2 permeance recovers to 370 GPU, and the H_2/CO_2 selectivity increases to 49, demonstrating the stability of the organosilica membranes.

Figure 9e compares H_2/CO_2 separation performance of several organosilica uTFC membranes with different PDMS layer thicknesses with other membranes. The POSi120 uTFC membrane

can have mixed-gas H_2 permeance of 910 GPU and H_2/CO_2 selectivity of 32 at 200 ºC, placing itself among the best-performing membranes for the H_2/CO_2 separation, which meets the targets for the BP2 (membranes with H_2 permeance of 500 GPU and H_2/CO_2 selectivity of 30).

6. FIELD TEST OF MEMBRANES WITH REAL SYNGAS

Design and Building Membrane Stamp Test Unit for Field Test at CAER of the University of Kentucky. The original plan was to conduct the field test at the National Carbon Capture Center (NCCC) by modifying a testing apparatus,[67] which MTR had used to test membrane stamps at NCCC. However, NCCC decided to discontinue the gasifier runs.

With the help from the DOE, we secured an agreement with the Center for Advanced Energy Research (CAER) at the University of Kentucky (UKy). We will join the field test with the campaign for the project "Zeolite Membrane Reactor for Pre-combustion Carbon Dioxide Capture" (FE0026435 with PI Jerry Lin at Arizona State University or ASU). Figure 10 shows the plan of the field test. The gasifier at CAER produced about 90 lb/h syngas, where 10 lb/h syngas was needed for the test in this project. As the ASU provided the majority of costs for running the gasifier, we can only run our system when the ASU unit was operating.

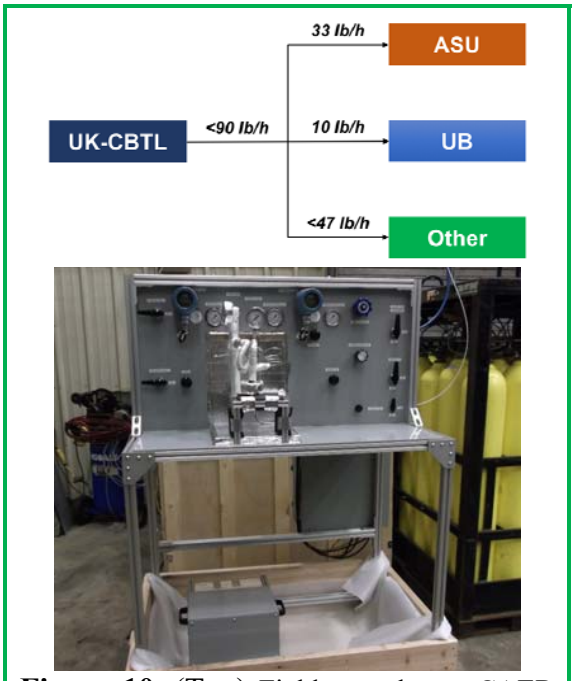

Figure 10. (Top) Field test plan at CAER of UKy. (b) Test skid designed and constructed by MTR at CAER.

With the new arrangement with the CAER, MTR cannot use the existing apparatus and had to design and build a testing unit that can operate in the syngas environment (Class I Div II). A photo of the skid is shown in Figure 10. will perform the field test for this project. The feed gas flow rate will be determined using a mass flow meter. A membrane test cell with a crossflow design will be used. The membrane stamps have an active area of 30 cm^2, while the stamps can be masked.

For the field tests, we prepared membrane stamps with effective areas larger than 1 cm^2 to get enough permeate gas flow rate for gas chromatography (GC) analysis. For example, the largest sample (#32) we prepared has an effective area of 2.88 cm^2, and exhibits a stable H_2 permeance of ~150 GPU and H_2/CO_2 selectivity of 43 in 20 h (Figure 11a). And the permeate H_2 flow rate is as high as ~7 standard cubic centimeters per minute (sccm) (Figure 11b).

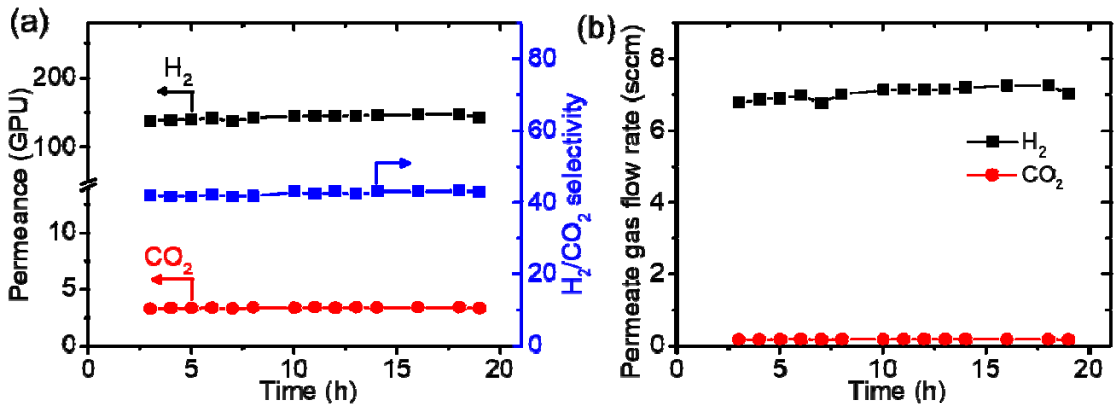

Figure 11. (a) Gas permeance and H_2/CO_2 selectivity, (b) permeate gas flow rate for sample #32 in mixed gas tests (H_2:CO_2 = 50:50) at 100 psig and 150 ºC.

Field Test Results. The typical composition of the syngas generated by CAER is listed in Table 4, and the pressure is about 350 psig. The feed syngas flow rate to our test system was kept between 40-50 slpm, and the feed gas pressure was controlled at 50-100 psig by a back pressure regulator.

Table 4. The typical composition of the syngas.

	H_2	N_2	CO	CO_2	H_2O	H_2S	COS
Content (%)	20.39	40.39	20.03	16.65	1.99	0.01	0.0049

During the field tests, we found the syngas could only be heated up to about 40 ºC because the gas heater unit is undersized. There was no sufficient time to order a new heater. Therefore, we can only run the exposure test for two membrane stamps. As shown in Figure 12, the membranes look intact after the field test, but the copper discs used to mask the membrane changed the color due to the reaction with the sulfur components in the syngas (H_2S or COS).

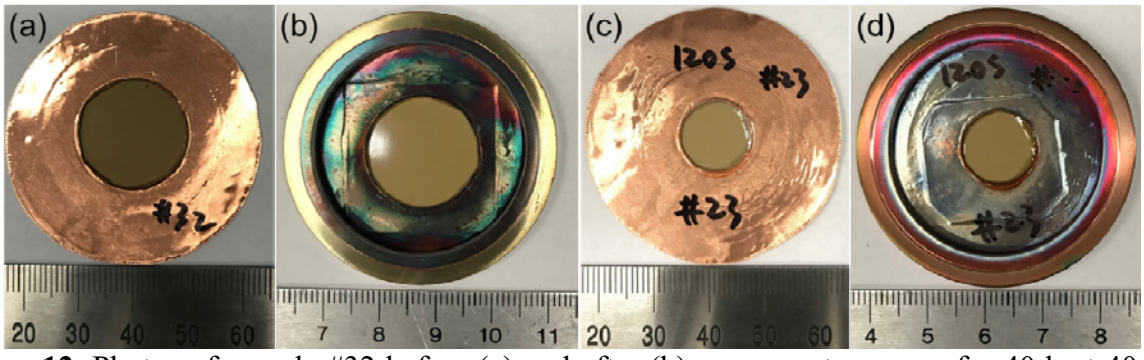

Figure 12. Photos of sample #32 before (a) and after (b) exposure to syngas for 40 h at 40 ºC; Photos of sample #23 before (a) and after (b) exposure to syngas for 22 h at 40 ºC.

Table 2 summarizes the gas separation performance of the two membrane stamps before and after the field test. For the sample #32, the H_2 permeance decreased slightly from 146 GPU to

114 GPU after the field test, while the CO_2 permeance increased significantly from 3.4 GPU to 9.3 GPU, leading to a decrease of H_2/CO_2 selectivity from 42 to 12. Membrane stamp #23 was accidentally broken during the test at UB after the field tests.

Table 5. Gas separation performance of the samples before and after the field test. All the tests were conducted in mixed gas (H_2:CO_2 = 50:50) at 100 psig and 150 ºC.

Samples	Before or after the field test	Temp. (ºC)	Permeance (GPU)		H_2/CO_2 selectivity
			H_2	CO_2	
#32	Before	150	146	3.4	42
#32	After	150	114	9.3	12
#23	Before	150	124	2.6	48
#23	After	60	7.5	1.3	5.8

7. PRODUCTS AND IMPACTS

During this project, four Ph.D. students received the inter-disciplinary training and graduated, including Shailesh Konda, Maryam Omidvar, Deqiang Yin, and Lingxiang Zhu. Two postdoctoral researchers (Dr. Liang Huang and Leiqing Hu) and two Ph.D. students (Abhishek Kumar and Hien Nguyen) are involved in this project.

The project leads to one provisional patent application, eight peer-reviewed articles, and one manuscript in preparation. The details are shown below.

1. Zhu, Huang, Swihart, and Lin, Organosilica Membranes, Methods of Making Same, and Uses Thereof, *Provisional patent application* filed on 1/17/2020
2. Zhu, Huang, Venna, Swihart, and Lin, Scalable Production of Few-Nanometer Organosilica Membranes for High-Temperature H_2/CO_2 Separation, *in preparation*
3. Omidvar, Nguyen, Huang, Doherty, Hill, Stafford, Feng, Swihart, and Lin, Unexpectedly Strong Size-Sieving Ability in Carbonized Polybenzimidazole for Membrane H_2/CO_2 Separation, *ACS Appl. Mater. & Interfaces*, 11 (50), 47365-47372 (2019)
4. Zhu, Yin, Qin, Konda, Zhang, Zhu, Liu, Xu, Swihart, and Lin, Sorption-Enhanced Mixed Matrix Membranes with Facilitated Hydrogen Transport for Hydrogen Purification and CO_2 Capture, *Adv. Funct. Mater.*, 1904357 (2019).
5. Omidvar, Stafford, and Lin, Thermally Stable Cross-linked P84 with Superior Membrane H_2/CO_2 Separation Properties at 100 ºC, *J. Membr. Sci.*, 575, 118-125 (2019)
6. Kumar, Mohammadi, and Swhart, Synthesis, growth mechanisms, and applications of palladium-based nanowires and other one-dimensional nanostructures, Nanoscale, 11, 19058 (2019)
7. Konda, Mohammadi, Buchner, Lin, and Swihart, Flame-based Synthesis and in situ Functionalization of Palladium Alloy Nanoparticles, *AIChE J.*, 64 (11), 3826-3834 (2018)

8. Omidvar, Nguyen, Liu, and Lin, Sorption-Enhanced Membrane Materials for Gas Separation: A Road Less Traveled, *Curr. Opin. Chem. Eng.*, 20, 50-9, 2018
9. Zhu, Swihart, and Lin, Unprecedented size-sieving ability in polybenzimidazole doped with polyprotic acids for membrane H_2/CO_2 separation, *Energy Environ. Sci.*, 11, 94-100 (2018)
10. Zhu, Swihart, and Lin, Tightening nanostructure of PBI for membrane H_2/CO_2 separation, *J. Mater. Chem. A*, 5, 19914-19923 (2017)

ATTACHMENT A -- State-Point Data for Membrane-Based Systems

	Units	Measured/ Estimated Performance	Projected Performance
Materials Properties			
Materials of Fabrication for Selective Layer		PBI/Pd MMMs	
Materials of Fabrication for Support Layer (if applicable)		PBI	
Nominal Thickness of Selective Layer (μm)		0.070	0.010
Membrane Geometry		Flat sheet	Flat sheet
Max Trans-Membrane Pressure	bar	15	40
Hours tested without significant degradation		120	120
Membrane Performance			
Temperature	°C	230	300
Pressure Normalized Flux for Permeate (H_2)	GPU or equivalent	400	500
H_2/N_2 Selectivity	-	132	132
H_2/CO_2 Selectivity	-	34	34
H_2/H_2O Selectivity	-	17	17
H_2/H_2S Selectivity	-	68	68
Type of Measurement (Ideal or mixed gas)	-	Mixed-gas	Mixed-gas
Proposed Module Design			
Flow Arrangement	-	Spiral wound membrane modules	
Packing Density	m^2/m^3	200 - 600	
Shell-Side Fluid	-	Syngas	

ATTACHMENT B -- State-Point Data for Membrane-Based Systems

	Units	Measured/ Estimated Performance	Projected Performance
Materials Properties			
Materials of Fabrication for Selective Layer		Silica on PDMS	
Materials of Fabrication for Support Layer (if applicable)		PBI	
Nominal Thickness of Selective Layer (μm)		0.010	0.010
Membrane Geometry		Flat sheet	Flat sheet or spiral wound
Max Trans-Membrane Pressure	bar	15	40
Hours tested without significant degradation		120	120
Membrane Performance			
Temperature	°C	200	200
Pressure Normalized Flux for Permeate (H_2)	GPU or equivalent	930	930
H_2/N_2 Selectivity	-	132	132
H_2/CO_2 Selectivity	-	33	33
H_2/H_2O Selectivity	-	17	17
H_2/H_2S Selectivity	-	66	66
Type of Measurement (Ideal or mixed gas)	-	Ideal-gas	Ideal-gas
Proposed Module Design			
Flow Arrangement	-	Spiral wound or hollow fiber	
Packing Density	m^2/m^3	300 – 1500	
Shell-Side Fluid	-	Raw syngas	

***Definitions for Table*:**

Membrane Geometry – flat discs or sheets, hollow fibers, tubes, etc.

Pressure Normalized Flux – For materials that display a linear dependence of flux on partial pressure differential, this is equivalent to the membrane's permeance.

GPU – Gas Permeation Unit, which is equivalent to 10^{-6} $cm^3/(cm^2 \cdot s \cdot cmHg)$ at 1 atm and 0 °C. For non-linear materials, the dimensional units reported shall be based on flux measured in $cm^3/(cm^2 \cdot s)$ (at 1 atm and 0 °C) with pressures measured in cm Hg. Note: 1 GPU = 3.3464×10^{-6} $kgmol/(m^2 \cdot s \cdot kPa)$ [SI units]

Type of Measurement – Either mixed or pure gas measurements; projected permeance and selectivities shall be for mixture of gases found in de-sulfurized flue gas or syngas.

Flow Arrangement – Typical gas-separation module designs include spiral-wound sheets, hollow-fiber bundles,

shell-and-tube, and plate-and-frame, which result in either co-current, counter-current, cross-flow arrangements, or some complex combination of these.

Packing Density – Ratio of the active surface area of the membrane to the volume of the module.

Shell-Side Fluid – Either the permeate or retentate stream.

References:

1. Figueroa, J. D.; Fout, T.; Plasynski, S.; McIlvried, H.; Srivastava, R. D., Advances in CO_2 capture technology - The U.S. Department of Energy's Carbon Sequestration Program. *Int. J. Greenh. Gas Con.* **2008,** *2*, 9-20.
2. *DOE NETL Report: Cost and Performance Baseline for Fossil Energy Plants (V 1): Bituminous Coal and Natural Gas to Electricity*. 2010.
3. Bell, D. A.; Towler, B. F.; Fan, M., *Coal gasification and its applications*. Elsevier Inc.: Oxford, UK, 2010.
4. Merkel, T. C.; Zhou, M.; Baker, R. W., Carbon dioxide capture with membranes at an IGCC power plant. *J. Membr. Sci.* **2012,** *389*, 441-450.
5. Bredesen, R.; Jordal, K.; Bolland, O., High-temperature membranes in power generation with CO_2 capture. *J. Membr. Sci.* **2004,** *43*, 1129-58.
6. Ma, Y.; Mardilovich, I. P.; Engwall, E. E., Thin composite palladium and palladium/alloy membranes for hydrogen separation. *Ann. N.Y. Acad. Sci.* **2003,** *984*, 346-360.
7. Ma, Y. H., Hydrogen Separation Membranes. In *Advanced Membrane Technology and Applications*, Li, N. N.; Fane, A. G.; Ho, W. S.; Matsuura, T., Eds. John Wiley & Sons: Hoboken, New Jersey, 2008; pp 671-684.
8. ConsERV Online Catalog. http://www.conserv.com/index.htm.
9. Baker, R. W., *Membrane Technology and Applications*. 3rd ed.; John Wiley and Sons, Ltd.: Chichester, UK, 2012.
10. Guazzone, F.; Catalano, J.; Mardilovich, I. P.; Kniep, J.; Pande, S.; Wu, T.; Lambrecht, R. C.; Datta, S.; Kazantzis, N. K.; Ma, Y. H., Gas permeation field tests of composite Pd and Pd-Au membranes in actual coal derived syngas atmosphere. *Int. J. Hydrogen Energ.* **2012,** *37*, 14557-14568.
11. Coulter, K. E.; Way, J. D.; Gade, S. K.; Chaudhari, S.; Alptekin, G. O.; DeVoss, S. J.; Paglieri, S. N.; Pledger, B., Sulfur tolerant PdAu and PdAuPt alloy hydrogen separation membranes. *J. Membr. Sci.* **2012,** *405*, 11-19.
12. Gade, S. K.; DeVoss, S. J.; Coulter, K. E.; Paglieri, S. N.; Alptekin, G. O.; Way, J. D., Palladium-gold membranes in mixed gas streams with hydrogen sulfide: Effect of alloy content and fabrication technique. *J. Membr. Sci.* **2011,** *378* (1-2), 35-41.
13. Hatlevik, O.; Gade, S. K.; Keeling, M. K.; Thoen, P. M.; Davidson, A. P.; Way, J. D., Palladium and palladium alloy membranes for hydrogen separation and production: History, fabrication strategies, and current performance. *Sep. Purif. Technol.* **2010,** *73* (1), 59-64.
14. Abdollahi, M.; Yu, J.; Liu, P. K. T.; Ciora, R.; Sahimi, M.; Tsotsis, T. T., Ultra-pure hydrogen production from reformate mixtures using a palladium membrane reactor system. *J. Membr. Sci.* **2012,** *390*, 32-42.
15. Parsley, D.; Ciora, R. J.; Flowers, D. L.; Laukaitaus, J.; Chen, A.; Liu, P. K. T.; Yu, J.; Sahimi, M.; Bonsu, A.; Tsotsis, T. T., Field evaluation of carbon molecular sieve membranes for the separation and purification of hydrogen from coal- and biomass-derived syngas. *J. Membr. Sci.* **2014,** *450*, 81-92.
16. Kniep, J.; Lin, Y. S., Effect of Zirconium doping on hydrogen permeation through Strontium Cerate Membranes. *Ind. Eng. Chem. Res.* **2010,** *49* (6), 2768-2774.
17. Liu, P. K.; Sahimi, M.; Tsotsis, T., Process intensification in hydrogen production from coal and biomass via the use of membrane-based reactive separations. *Curr. Opin. Chem. Eng.* **2012,** *1*, 342-351.

18. Merkel, T.; Zhou, M.; Thomas, S.; Lin, H.; Serbanescu-Martin, A.; Amo, K. D. In *Novel polymer membranes for pre-combustion CO_2 capture from coal-derived syngas*, NETL CO_2 Capture Technology Meeting, Pitttsburgh, PA, August 26, 2011; Pitttsburgh, PA, 2011.
19. Poling, B. E.; Prausnitz, J. M.; O'Connell, J. P., *The Properties of Gases and Liquids*. 5th ed.; McGraw-Hill: New York, 2000.
20. Breck, D. W., *Zeolite Molecular Sieves*. Krieger Publishing Company: Florida, 1974.
21. Freeman, B. D., Basis of permeability/selectivity tradeoff relations in polymeric gas separation membranes. *Macromolecules* **1999,** *32* (2), 375-380.
22. Lin, H.; Van Wagner, E.; Freeman, B. D.; Toy, L. G.; Gupta, R. P., Plasticization-enhanced H_2 purification using polymeric membranes. *Science* **2006,** *311* (5761), 639-642.
23. Lin, H.; Freeman, B. D., Materials selection guidelines for membranes that remove CO_2 from gas mixtures. *J. Mol. Struct.* **2005,** *739* (1-3), 57-74.
24. Robeson, L. M., The upper bound revisited. *J. Membr. Sci.* **2008,** *320*, 390-400.
25. Robeson, L. M., Correlation of separation factor versus permeability for polymeric membranes. *J. Membr. Sci.* **1991,** *62*, 165-185.
26. Berchtold, K. A.; Singh, R. P.; Young, J. S.; Dudeck, K. W., Polybenzimidazole composite membranes for high temperature synthesis gas separations. *J. Membr. Sci.* **2012,** *415-416*, 265-270.
27. Jorgensen, B. S.; Young, J. S.; Espinoza, B. F. Cross-linked polybenzimidazole membrane for gas separation. US 6,946,015, 2006.
28. Chung, T. S.; Shao, L.; Tin, P. S., Surface modification of polyimide membranes by diamines for H_2 and CO_2 separation. *Macromol. Rapid Commun.* **2006,** *27*, 998-1003.
29. Shao, L.; Low, B. T.; Chung, T. S.; Greenberg, A. R., Polymeric membranes for the hydrogen economy: Contemporary approaches and prospects for the future. *J. Membr. Sci.* **2009,** *327*, 18-31.
30. Low, B. T.; Chung, T. S.; Chen, H. M.; Jean, Y. C.; Pramoda, K. P., Tuning the Free Volume Cavities of Polyimide Membranes via the Construction of Pseudo-Interpenetrating Networks for Enhanced Gas Separation Performance. *Macromolecules* **2009,** *42* (18), 7042-7054.
31. Low, B. T.; Xiao, Y. C.; Chung, T. S., Amplifying the molecular sieving capability of polyimide membranes via coupling of diamine networking and molecular architecture. *Polymer* **2009,** *50* (14), 3250-3258.
32. Krishnan, G.; Jayaweera, I.; Bhamidi, S.; Nagar, A.; Sanjurjo, A.; Callahan, R.; BoBrien, K. In *Fabrication and scale-up of polybenzimidazole (PBI) membrane based system for precombustion based capture of carbon dioxide*, NETL CO_2 Capture Technology Conference, Pittsburgh, PA, Pittsburgh, PA, 2011.
33. Krishnan, G. In *Development of a precombustion CO_2 capture process using high-temperature PBI hollow-fiber membranes*, NETL CO_2 Capture Technology Meeting, Pittsburgh, PA, Pittsburgh, PA, 2014.
34. Kim, H. W.; Yoon, H. W.; Yoon, S. M.; Yoo, B. M.; Ahn, B. K.; Cho, Y. H.; Shin, H. J.; Yang, H.; Paik, U.; Kwon, S.; Choi, J. Y.; Park, H. B., Selective gas gransport through few-layered graphene and graphene oxide membranes. *Science* **2013,** *342* (6154), 91-95.
35. Li, H.; Song, Z. N.; Zhang, X. J.; Huang, Y.; Li, S. G.; Mao, Y. T.; Ploehn, H. J.; Bao, Y.; Yu, M., Ultrathin, molecular-sieving graphene oxide membranes for selective hydrogen separation. *Science* **2013,** *342* (6154), 95-98.

36. Brown, A. J.; Brunelli, N. A.; Eum, K.; Rashidi, F.; Johnson, J. R.; Koros, W. J.; Jones, C. W.; Nair, S., Interfacial microfluidic processing of metal-organic framework hollow fiber membranes. *Science* **2014,** *345* (6192), 72-75.
37. Lin, H.; Yavari, M., Upper bound of polymeric membranes for mixed-gas CO_2/CH_4 separations. *J. Membr. Sci.* **2015,** *475*, 101-109.
38. Adams, B. D.; Chen, A. C., The role of palladium in a hydrogen economy. *Materials Today* **2011,** *14* (6), 282-289.
39. Kalidindi, S. B.; Oh, H.; Hirscher, M.; Esken, D.; Wiktor, C.; Turner, S.; Tendeloo, G.; Fischer, R. A., Metal-COFs: Covalent Organic Frameworks as Templates for Pd Nanoparticles and Hydrogen Storage Properties of Pd-COF-102 Hybrid Material. *Chem. Eur. J.* **2012,** *18* (35), 10848-10856.
40. Kalidindi, S. B.; Fischer, R. A., Covalent organic frameworks and their metal nanoparticle composites: Prospects for hydrogen storage. *Phys. Status Solidi B* **2013,** *250* (6), 1119-1127.
41. Matsunaga, S.; Endo, N.; Mori, W., Microporous Porphyrin-Based Metal Carboxylate Frameworks with Various Accessible Metal Sites: Cu2(MDDCPP) M=Zn2+, Ni2+, Pd2+, Mn3+(NO3), Ru2+(CO). *Eur. J. Inorg. Chem.* **2012,** (30), 4885-4897.
42. Mendoza-Cortes, J. L.; Goddard, W. A.; Furukawa, H.; Yaghi, O. M., A Covalent Organic Framework that Exceeds the DOE 2015 Volumetric Target for H-2 Uptake at 298 K. *J. Phys. Chem. Lett.* **2012,** *3* (18), 2671-2675.
43. Smith, Z. P.; Tiwari, R. R.; Murphy, T. M.; Sanders, D. F.; Gleason, K. L.; Paul, D. R.; Freeman, B. D., Hydrogen sorption in polymers for membrane applications. *Polymer* **2013,** *54* (12), 3026-3037.
44. Merkel, T. C.; Bondar, V. I.; Nagai, K.; Freeman, B. D.; Pinnau, I., Gas Sorption, Diffusion, and Permeation in Poly(dimethylsiloxane). *J. Polym. Sci. B: Polym. Phys.* **2000,** *38*, 415-434.
45. Ghosal, K.; Chern, R. T.; Freeman, B. D.; Daly, W. H.; Negulescu, I. I., Effect of basic substituents on gas sorption and permeation in polysulfone. *Macromolecules* **1996,** *29*, 4360-4369.
46. Horn, N. R.; Paul, D. R., Carbon dioxide sorption and plasticization of thin glassy polymer films tracked by optical methods. *Macromolecules* **2012,** *45* (6), 2820-2834.
47. Merkel, T. C.; Bondar, V.; Nagai, K.; Freeman, B. D.; Yampolskii, Y. P., Gas Sorption, Diffusion, and Permeation in Poly(2,2-bis(trifluoromethyl)-4,5-difluoro-1,3-dioxole-co-tetraflroroethylene). *Macromolecules* **1999,** *32*, 8427-8440.
48. Merkel, T. C.; Bondar, V.; Nagai, K.; Freeman, B. D., Sorption and transport of hydrocarbon and perfluorocarbon gases in poly(1-trimethylsilyl-1-propyne). *J. Polym. Sci. Part B: Polym. Phys.* **2000,** *38* (2), 273-296.
49. Pinnau, I.; Toy, L. G., Solid polymer electrolyte composite membranes for olefin/paraffin separation. *J. Membr. Sci.* **2001,** *184*, 39-48.
50. Ramasubramanian, K.; Zhao, Y.; Ho, W. S., CO_2 capture and H_2 purification: Prospects for CO_2-selective membrane processes. *AIChE J.* **2013,** *59* (4), 1033-1045.
51. Chung, T. S.; Jiang, L. Y.; Li, Y.; Kulprathipanja, S., Mixed matrix membranes (MMMs) comprising organic polymers with dispersed inorganic fillers for gas separation. *Progr. Polym. Sci.* **2007,** *32* (4), 483-507.
52. Vu, D. Q.; Koros, W. J.; Miller, S. J., High Pressure CO_2/CH_4 Separation Using Carbon Molecular Sieve Hollow Fiber Membranes. *Ind. Eng. Chem. Res.* **2002,** *41*, 367-380.

53. Koros, W. J.; Lively, R. P., Water and beyond: Expanding the spectrum of large-scale energy efficient separation processes. *AIChE J.* **2012,** *58* (9), 2624-2633.
54. Merkel, T. C.; Freeman, B. D.; Spontak, R. J.; He, Z.; Pinnau, I.; Meakin, P.; Hill, A. J., Ultrapermeable, Reverse-Selective Nanocomposite Membranes. *Science* **2002,** *296*, 519-522.
55. Vu, D. Q.; Koros, W. J.; Miller, S. J., Mixed matrix membranes using carbon molecular sieves - I. Preparation and experimental results. *J. Membr. Sci.* **2003,** *211* (2), 311-334.
56. Ordonez, M. J. C.; Balkus, K. J.; Ferraris, J. P.; Musselman, I. H., Molecular sieving realized with ZIF-8/Matrimid (R) mixed-matrix membranes. *J. Membr. Sci.* **2010,** *361* (1-2), 28-37.
57. Perez, E. V.; Balkus, K. J.; Ferraris, J. P.; Musselman, I. H., Mixed-matrix membranes containing MOF-5 for gas separations. *J. Membr. Sci.* **2009,** *328* (1-2), 165-173.
58. Adams, R.; Carson, C.; Ward, J.; Tannenbaum, R.; Koros, W., Metal organic framework mixed matrix membranes for gas separations. *Microporous Mesoporous Mater.* **2010,** *131* (1-3), 13-20.
59. Bae, T. H.; Lee, J. S.; Qiu, W. L.; Koros, W. J.; Jones, C. W.; Nair, S., A High-Performance Gas-Separation Membrane Containing Submicrometer-Sized Metal-Organic Framework Crystals. *Angew. Chem. Inter. Ed.* **2010,** *49* (51), 9863-9866.
60. Kattula, M.; Ponnuru, K.; Zhu, L.; Jia, W.; Lin, H.; Furlani, E. P., Designing ultrathin film composite membranes: The impact of a gutter layer. *Sci. Rep.* **2015,** *5*, 15016.
61. Zhu, L. X.; Yavari, M.; Jia, W. G.; Furlani, E. P.; Lin, H. Q., Geometric Restriction of Gas Permeance in Ultrathin Film Composite Membranes Evaluated Using an Integrated Experimental and Modeling Approach. *Ind. Eng. Chem. Res.* **2017,** *56* (1), 351-358.
62. Ferguson, G. S.; Chaudhury, M. K.; Sigal, G. B.; Whitesides, G. M., Contact Adhesion of Thin Gold Films on Elastomeric Supports: Cold Welding Under Ambient Conditions. *Science* **1991,** *253* (5021), 776.
63. Owen, M. J.; Smith, P. J., Plasma treatment of polydimethylsiloxane. *J. Adhes. Sci. Techn.* **1994,** *8* (10), 1063-1075.
64. Hillborg, H.; Ankner, J. F.; Gedde, U. W.; Smith, G. D.; Yasuda, H. K.; Wikström, K., Crosslinked polydimethylsiloxane exposed to oxygen plasma studied by neutron reflectometry and other surface specific techniques. *Polymer* **2000,** *41* (18), 6851-6863.
65. Béfahy, S.; Lipnik, P.; Pardoen, T.; Nascimento, C.; Patris, B.; Bertrand, P.; Yunus, S., Thickness and Elastic Modulus of Plasma Treated PDMS Silica-like Surface Layer. *Langmuir* **2010,** *26* (5), 3372-3375.
66. Matsuyama, H.; Teramoto, M.; Hirai, K., Effect of plasma treatment on CO_2 permeability and selectivity of poly(dimethylsiloxane) membrane. *J. Membr. Sci.* **1995,** *99* (2), 139-147.
67. Merkel, T.; Zhou, M.; Thomas, S.; Lin, H.; Serbanescu-Martin, A.; Vu, J.; Amo, K. D.; Wagener, E. H.; Jin, J.; Haldeman, A.; Klep, V.; Wu, T.; Wheeldon, J.; Datta, S.; Robert, C. *Novel polymer membrane process for pre-combustion CO_2 capture from coal-derived syngas (DE-FE0001124), Final report to the DU.S. Department of Energy*; Membrane Technology and Research, Inc.: 2011.